Adverse Effects in Dual-Feed Interferometry

M. Mark Colavita

Jet Propulsion Laboratory, California Institute of Technology
4800 Oak Grove Dr., Pasadena, CA 91109 USA

Abstract

Narrow-angle dual-star interferometric astrometry can provide very high accuracy in the presence of the Earth's turbulent atmosphere. However, to exploit the high atmospherically-limited accuracy requires control of systematic errors in measurement of the interferometer baseline, internal OPDs, and fringe phase. In addition, as high photometric SNR is required, care must be taken to maximize throughput and coherence to obtain high accuracy on faint stars. This article reviews the key aspects of the dual-star approach and implementation, the main contributors to the systematic error budget, and the coherence terms in the photometric error budget.

Key words: interferometry, astrometry, dual-star, phase referencing

1 Introduction

1.1 Astrometry with interferometers

Figure 1 illustrates the fundamental astrometric geometry of a Michelson interferometer. Fringes are detected when the external path delay is equal to the internal path delay. While the former cannot be directly measured, the latter can be directly measured with a laser distance gauge. The accuracy of this measurement is one contributor to the achieved astrometric accuracy. For ground-based astrometry, the requirement is usually on differential accuracy as one switches between target and calibrator stars, and applies for the duration of the specific measurement sequence.

If the baseline $\vec{B}$ is taken to be the vector connecting the pivots of the two collectors, then the delay x is given as

$$x = \vec{B} \cdot \hat{s} + c, \tag{1}$$

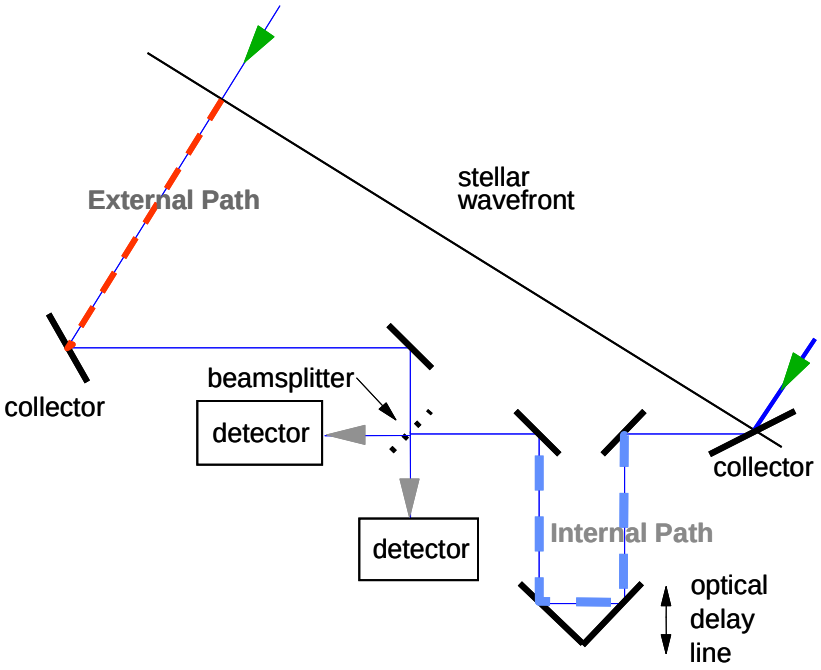

Figure 1. Detecting fringes with an interferometer.

where $\hat{s}$ is the star unit vector, and c is the "constant" term, sometimes incorporated into the delay. Strictly, this geometric equation describes the non-measurable "external delay;" astrometric errors arise when we try to estimate the external delay via the internal delay and the fringe residual. These errors can include laser metrology accuracy and its correlation with the starlight path; fringe measurement accuracy, including SNR; and internal atmospheric and dispersive effects. The other terms in Eq. 1 also impact accuracy, including atmospheric noise and classical refraction that can affect $\hat{s}$, and knowledge and stability of $\vec{B}$.

1.2 Atmospheric limit to narrow-angle astrometry

Consider a differential astrometric measurement as illustrated in Fig. 2. Astrometric noise arises as rays from different stars separated by angle θ traverse different paths through the atmosphere. Intuitively, one would expect the error to depend on the separation of the beams in the atmosphere, θh, where h is the atmospheric height, as well as on the amount of overlap of the beams with respect to instrument extent, B, which would be the telescope diameter, for a single-telescope measurement, or the interferometer baseline, which is of interest here. This intuition is indeed correct, and the error behavior becomes very favorable when $\theta h < B$ (Shao & Colavita, 1992).

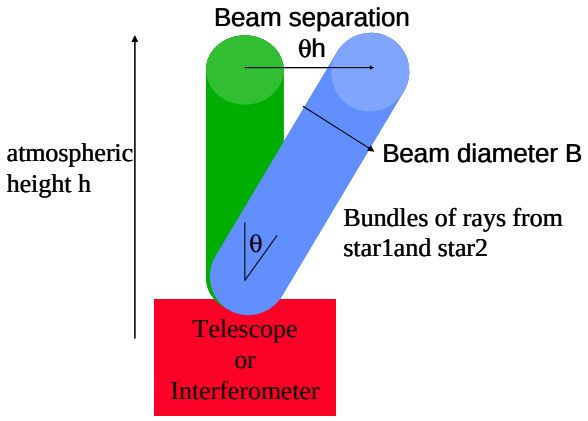

Figure 2. Schematic differential measurement.

The detailed behavior is shown in Fig. 3. In the very-narrow-angle case, where $\theta h << B$, the error takes the form

$$\epsilon(T) \propto B^{-2/3}\theta \left(\int dh C_n^2(h) h^2 \right)^{1/2} T^{-1/2}, \tag{2}$$

or evaluated for a Mauna Kea turbulence profile,

$$\epsilon(T) \simeq 300 B^{-2/3}\theta T^{-1/2}. \tag{3}$$

Of note is that the error is white, i.e., the standard deviation improves with the square root of the integration time. In addition, the standard deviation is linear with star separation and has a nearly inverse baseline dependence. Note also, compared to the usual seeing metric r_0 which involves a straight integral over the turbulence profile, the narrow-angle expression weights high altitude turbulence as h^2. The expression above uses an infinite-outer-scale Kolmogorov atmospheric model. With a finite outer scale, the error dependence changes from $\theta B^{-2/3}$ to $\theta L_0^{1/3} B^{-1}$. As an example, for a Mauna Kea turbulence profile, $\theta = 15$ arcsec, and $L_0 = 40$ m, the error in a T = 1000 sec integration time is $\sim$24 μas for a 100 m baseline; and $\sim$12 μas for a 200 m baseline. These are very interesting performance levels.

1.3 Implementing a dual-star interferometer

Thus with the long baseline of an interferometer, ten's of microarcsecond accuracy is possible for measurements made over small fields. In addition, over small fields, the requirements on baseline knowledge are greatly decreased. However, the measurements of the two stars must be essentially simultaneous

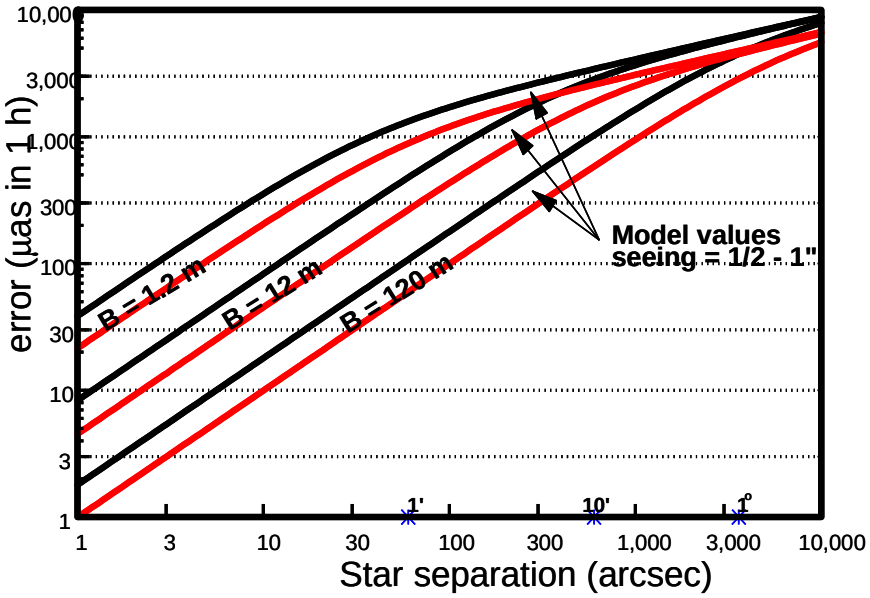

Figure 3. Limits to a narrow-angle astrometric measurement.

in order to exploit the common-mode nature of the atmosphere over small fields. A practical consideration is that small fields mean that the second star will be faint. Another practical consideration is that interferometers usually pass only small fields of view. Thus a simultaneous differential measurement will require the instrument to simultaneously observe two separate fields of view. This will require an instrument with two separate beam trains, as well as laser metrology to "tie" the two beam trains together.

These considerations lead to the dual-star approach (Shao & Colavita, 1992), illustrated schematically in Fig. 4. The keys aspects of the dual-star approach are:

- Two interferometers, sharing a common baseline and apertures, with laser metrology to tie them together
- Two stars: one bright (target, nearby); one faint (astrometric reference, distant)
- Observe target star on first interferometer
  - Use as phase reference for stars within its isoplanatic patch; feedforward to second interferometer
- Observe astrometric reference star on second interferometer
- Work in the infrared (2.2 μm) for its larger isoplanatic angle
  - Increases solid angle over which to find astrometric reference stars ($\sim$20 arcsec radius)
- Use 2 m class, or larger, apertures to provide sensitivity for adequate sky

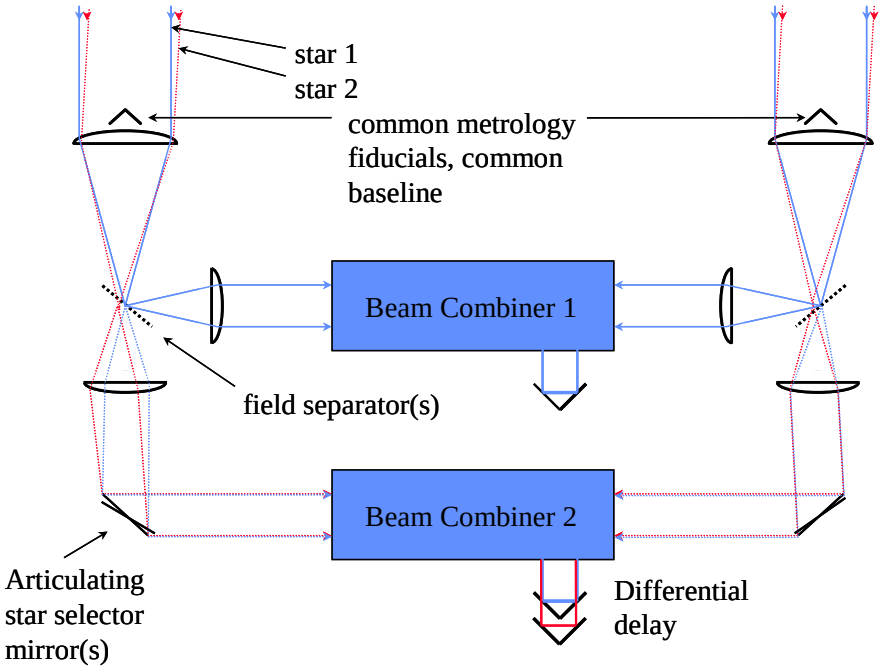

Figure 4. Dual-star optical concept.

coverage for astrometric reference stars.

· AO ($D > 2$ m) or fast tip/tilt ($D < 2$ m) needed to correct aperture

Operationally, beam combiner 1 continually tracks the bright star, providing the necessary phase referencing. Beam combiner 2 makes the differential measurement, switching between the bright and faint stars. Implications in this operational scenario on the implementation are that beam combiners 1 and 2 can be different; metrology continuity (or absolute metrology) is required; and that the star separator has to pass both stars. Other dual-star approaches are possible; this concept follows from the implementation at PTI (Colavita et al., 1999), and what had been planned for the proposed Keck Interferometer outrigger project (cf. Hrynevych, Ligon, & Colavita, 2004).

2 Systematic errors

Perhaps surprisingly, the random atmospheric noise will likely be the least bothersome term in the end-to-end dual-star error budget. In addition, the finite SNR of the measurement will be quite important, as the small fields allowed by phase referencing require faint reference stars. However, astrometry is very much about the control of systematic errors, and we discuss that below.

A simple two-dimensional sensitivity analysis is useful in understanding the

requirements. We can write the astrometric equation for a differential measurement, following Eq. 1, as

$$\Delta x = \vec{B} \cdot \Delta \hat{s}. \tag{4}$$

We can rewrite this in two dimensions for estimating the differential angle θ in terms of length l, phase ϕ, baseline B as

$$l + k^{-1}\phi = B\theta, \tag{5}$$

for which a simple sensitivity analysis illustrates the required accuracies:

$$\delta\theta = \frac{\delta l}{B} + \frac{k^{-1}\delta\phi}{B} - \frac{\delta B}{B}\theta. \tag{6}$$

These three terms are OPD measurement noise δl, fringe measurement noise $\delta\phi$, and baseline noise δB. Each of these three terms depends inversely on baseline; in addition, the baseline term is proportional to field-of view.

For the purpose of the following discussion, assume $\lambda = 2.2$ μm, $\theta = 15$–20 arcsec and $B = 100$ m. Longer baselines are better both for the atmospheric term, as well as for the systematic terms in Eq. 6; in practice, the baseline should be made a long as possible, limited by the finite size of the phase-reference star. Assume our desired accuracy is $\delta\theta = 20$ μas, and that we allocate 10 μas to each of the three terms in Eq. 6. Then, $\delta B = 50$ μm rms, and $\delta l = \delta\phi = 5$ nm rms.

Below, we do some example suballocations to give a feel for what terms are important. We also identify mechanisms by which systematic errors get introduced, the magnitudes of the underlying effects, and approaches for mitigating these effects. We describe these three terms below, starting with the baseline term.

2.1 Baseline noise

For the assumptions above, the required baseline knowledge is $\delta B = B(d\theta/\theta)$ $= 50$ μm. We suballocate this amount among the following four terms at 25 μm each.

2.1.1 Wide-angle baseline solution

Solving for the wide-angle baseline is a standard task in order to find fringes with an interferometer. The 25 μm requirement corresponds to 50 mas for our assumed 100 m baseline. The contributors are:

a) Input star position accuracy: ∼20 mas. The Hipparcos catalog (Perryman, Lindegren, Kovalevsky, et al., 1997) is the usual source of positions for the bright stars (it's complete to V = 7.3) used in a baseline solution. The accuracy of the catalog today is determined by propagation of errors in the proper motion estimates. Given positional accuracies of 1–3 mas for epoch 1991.25 and proper motion accuracy of 1–2 mas/yr, we should be able to assume typical accuracies of 20 mas for epoch 2010 (Zacharias et al., 2004).

b) Wide-angle atmospheric accuracy: <50 mas. For $L_0 \ll B$, the fringe position fluctuations are given by (cf. Roddier, 1981)

$$\sigma_x \simeq 0.42\lambda \left(\frac{L_0}{r_0}\right)^{5/6}. \tag{7}$$

For an $L_0 = 40$ m outer scale and $r_0 = 20$ ms ($\frac{1}{2}$ arcsec seeing), $\sigma_x = 20$ μm rms, or 40 mas rms with a 100 m baseline. With a correlation time of L_0/W for wind speed W, this should average down for a typical integration time.

c) DCR: < 1 μm. For a telescope, DCR (differential chromatic refraction) refers to image elongation along the zenith direction attributable to the wavelength dependence of the atmospheric refractivity. For an interferometer, in the limit of a plane-parallel atmospheric, there is in principle no DCR if internal OPDs are measured at the same wavelength as the science measurement (or if the delay lines are in vacuum, as this is usually expressed). The extent to which the science and metrology wavelengths differ, and the dispersion characteristics of the atmosphere, set the size of this term. While it's not significant for wide-angle astrometry, we'll return to it below in the context of OPD measurement errors.

2.1.2 Unmodeled baseline noise

This term in the baseline-noise budget addresses the "mechanical" quality of the wide-angle baseline. It's the noise in the telescope pivots that is unaccounted for in the wide-angle baseline solution. We allocate 25 μm total to this term; 17 μm per telescope. This term of the error budget is a knowledge requirement – the values refer only to the unmodelable component – and thus it includes terms such as non-repeatable bearing noise, unmodeled flexure, and thermal deformation. In practice this term should be manageable with good

telescope design and an appropriate modeling strategy. An existence proof would be measurements made of pivot quality of one of the Keck Interferometer outrigger telescopes (Hrynevych, Ligon, & Colavita, 2004). After fitting the measured azimuth and elevation runouts to fourth-order harmonic models, the residual per telescope was $\sim$10 μm rms.

2.1.3 Wide-angle baseline identification

Understanding the 25 μm allocation to this term requires an understanding of what defines the narrow-angle baseline, i.e., the baseline that applies to the narrow-angle measurement. Recall the dual-star optical concept from Fig. 4. While for wide-angle astrometry we articulate between stars by repointing the telescopes, for narrow-angle astrometry we articulate between stars by tilting a mirror in the star separators. There's no a priori reason why these baselines should be the same, i.e., the wide-angle baseline we carefully solved for above may be unrelated to the narrow-angle baseline that we really care about.

Normally the wide-angle baseline is defined as connecting the telescope pivot points as illustrated in Fig. 5(a). However, providing OPD measurements with adequate accuracy for narrow-angle astrometry will require end-to-end, or nearly end-to-end, laser metrology: how does this affect the baseline definition?

Consider Fig. 5(b), which shows the metrology corner cubes (assumed subaperture) located at the telescope pivots, and accessible by both dual-star beam combiners. In this case, the wide-angle and narrow-angle baselines are the same, leaving only one error term: the accuracy in locating the fiducial on the pivot. However, it's not necessarily the case that the actual pivot is accessible this way.

However, with reference to Fig. 5(c), it turns out that we can put the corner cubes anywhere in input space (i.e., prior to the first optic), as long as we define the baseline as the vector connecting the vertices of the corner cubes. However, two questions – and two contributors the error budget – remain: a) how do you ensure that this new baseline is also the one solved for earlier; b) how do you ensure that this is also the narrow-angle baseline?

2.1.4 Narrow-angle to wide-angle baseline transfer

Ideally, one would solve for the narrow-angle baseline directly, analogously to solving for the wide-angle baseline. Unfortunately, this is not generally possible, as ten's of microarcseconds a priori astrometric accuracy would be required for these stars (although in principle some sort of ratiometric approach using reference narrow-angle pairs is not excluded). We describe below the approach for determining the narrow-angle baseline that was planned for the proposed

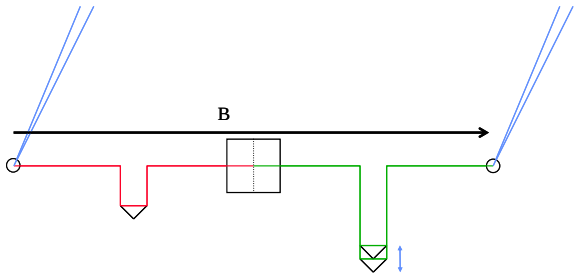

(a)

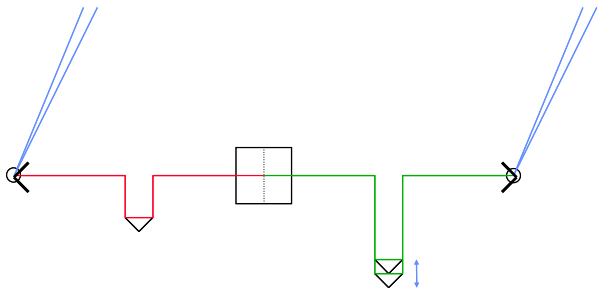

(b)

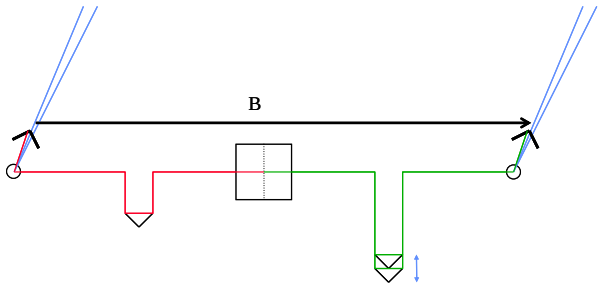

(c)

Figure 5. Definition of the wide-angle baseline.

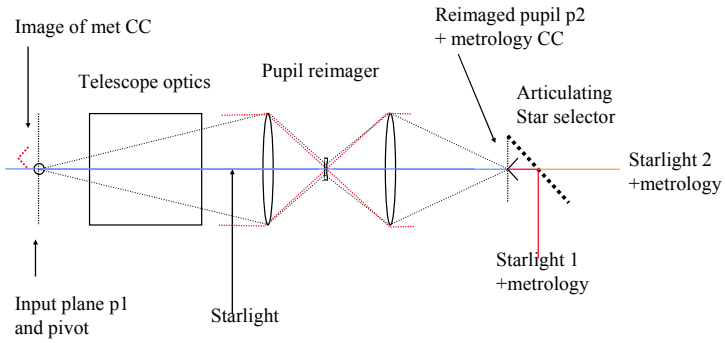

Figure 6. Schematic star separator.

Keck Interferometer outrigger project (Hrynevych, Ligon, & Colavita, 2004).

The approach used a pivot beacon near the real pivot (conceptually, located at the tertiary surface but in input space). Using an auxiliary measurement system, this pivot beacon would be surveyed as the telescope was articulated, in order to transfer the beacon to the wide-angle baseline. Inside the star selector, a metrology corner cube would be aligned to an image of the beacon in order to define the narrow-angle baseline.

Figure 6 shows a schematic star separator for a large telescope. From left to right is the physical telescope pivot in the entrance pupil p_1, which precedes the first optic in the system (nominally in the plane of the tertiary). The box "Telescope Optics" includes all of the optics from the entrance pupil to the star selector. The pupil reimager – part of the star separator – images the entrance pupil to the plane p_2, which includes the metrology corner cube that ties together the two beam combiners. Also in this plane (or very close to it) is an articulating star selector, in this implementation realized as an articulating beamsplitter, which reflects one star and transmits the other.

If the pupil reimaging is exact, the metrology corner cube is projected onto the pivot (or more precisely, onto a pivot beacon which has been tied to the pivot), and this transfer ties the narrow-angle baseline to the wide-angle baseline subject to some caveats. In principle, this transfer can be aided by a camera on the beam-combiner side of star selector which images the conjugate planes

p_1 and p_2, along with illumination of the metrology corner cube and pivot beacon. The caveats include acceptable control of beamwalk and aberration in the pupil reimager and in the telescope optics, as well as control of tolerances in the reimaging. The tolerancing on the transfer uses the wide-angle tolerances, i.e., the lateral mapping must be done with 25 μm accuracy. There is also a relatively loose longitudinal tolerance δz: we require $(1/2)\theta^2 \delta z \ll 5$ nm, which requires $\delta z \ll 1$ m.

2.2 OPD measurement noise

OPD measurement noise δl refers to errors in measuring the "internal pathlength" of Fig. 1, to which we had allocated 5 nm above. The sources of error in this measurement include laser metrology accuracy, beam walk errors, thermal stability, DCR (mostly from air, but also other dispersive material), and environmental stability.

2.2.1 Laser metrology accuracy

To first order, if one wanted to keep this portion of the measurement noise term to 1 nm over the 100 m pathlengths within the interferometer, laser metrology accuracy of 10^{-11} would be required. While this level is possible, commonly-used stabilized lasers have accuracy $\sim 10^{-8}$. However, it is possible to design the instrument such that the metrology need only be accurate over the ten's of mm of OPD articulation range as one switches between stars, in which case the required accuracy is now $\sim 10^{-7}$. One way to achieve this is to use the same laser source for all of the metrology beams, in which case errors in the large common-mode paths of primary and secondary drop out.

2.2.2 Beam walk

As we're worried about system accuracies of nanometers, we need to account for the fact that optical surfaces are not smooth at the nanometer level. A $\lambda/20$ surface in reflection introduces a wavefront error across the optic of $\sim$13 nm rms; 16 such surfaces in series, assuming RSS combination, leads to 50 nm rms errors. If these effects are static, they just impact Strehl. However for astrometry, this wavefront error can introduce errors when beams walk across the optics. While thermal drift and seeing compensation can introduce beam walk, it also gets introduced when switching between stars in the star selector. With reference to Fig. 6, for which the star selector mirror is conjugate to the input pupil, as the star selector mirror is articulated, there will be beam walk on the telescope optics.

The error from beam walk can show up in two ways. One is from changes in an unmonitored path as a beam walks; the second is from differences between the path seen by starlight, which typically represents an average of the wavefront over a large diameter, vs. the path seen by laser metrology, which will typically be subaperture and sample a much smaller fraction of the wavefront.

One can do a stochastic analysis of the problem (see the Appendix). Subject to a number of assumptions, the rms beam walk error ϵ can be approximated as (see Eqs. A.16 & A.21; we round down the leading coefficient)

$$\epsilon \sim w \left(\frac{\Delta^*}{q^*}\right) \left(\frac{q^*}{Z^*}\right)^{0.25}, \Delta^* \ll q^*, \tag{8}$$

where w is the total rms wavefront over an optic of diameter Z^*, Δ^* is the transverse beam walk, and q^* is diameter of the footprint of the illumination on the optic. If $q^* = D^*$, where D^* is the diameter of the starlight footprint, Eq. 8 gives the change in OPD as the beam translates by a distance Δ^*. Alternatively, if $q^* = d^*$, where d^* is the diameter of a subaperture metrology beam in the middle of the starlight beam, $d^* \ll D^*$, then Eq. 8 gives the error caused by different sampling of the wavefront by the metrology vs. the starlight as the beams translate, together, by distance Δ^*.

As an example, consider a $Z^* = 20$ cm optic with $w = 50$ nm rms (representing 16 optics in series, as described above), a metrology diameter $d^* = 2$ cm (small compared to an assumed starlight diameter $D^* = 10$ cm), and a shear $\Delta^* = 1$ cm: Eq. 8 predicts an error $\sim$15 nm rms, which is $\sim$5$\times$ larger than the estimated change in OPD seen by the starlight footprint. This analysis is very approximate, but illustrates the nature of the issue, and the perhaps surprising result that metrology of a common mode path subject to beamwalk can introduce errors. Note that large aspheres can have significant zonal errors, which could be a larger effect than that given above; on the other hand, in smaller diameters, superpolished ($\lambda/100$) optics are available which could be useful for critical locations where the relative beamwalk is large.

2.2.3 Thermal stability

Even if you meter everything, you still need to introduce the metrology into the starlight path in a way that doesn't introduce its own complications. As an example, suppose you introduce the metrology from behind the starlight beamsplitter into the center of pupil, but add two small polarizers in the center of the beam which are seen by just the metrology. How stable do these non-common optics need to be?

The thermo-optical constant G measures the change in OPD with temperature

as an optic changes in size and refractivity, viz. $G \approx N \times \mathrm{CTE} + dN/dT$, where CTE is the ordinary coefficient of thermal expansion and N is refractivity, $N = n-1$. As an example, BK7, a common optical glass, has $G = 7\times10^{-6}$, such that a 10 mm thickness introduces an OPD error of 70 nm K^{-1}. While better glasses exist, it is better to design out the problem. One way is an approach with no non-common optics; another is to design the observation scenario such that stability is only required over a short switching timescale. The latter approach, using the design of the observational scenario, is helpful for dealing with many sorts of systematic errors, including those we'll be discussing below.

2.2.4 Differential chromatic refraction (DCR)

While vacuum delay lines (and vacuum beam pipes), in principle, make most of this problem go away (leaving only a small second order term due to curvature of the Earth), many interferometers use air delay lines, and are thus sensitive to the dispersion of air in the internal interferometer paths. Consider the effect of star color. The change in refractivity (Ciddor, 1996) of dry air at 1 atmosphere is $\Delta N \approx 3.0 \times 10^{-9}$ between $\lambda = 2.20$ μm and 2.21 μm, i.e., for a $\delta\lambda = 10$ nm wavelength uncertainty. For 100 m of total pathlength, this corresponds to an error of 300 nm, which is much larger than our allocation of 5 nm for all measurement errors. To first order, the implication appears to be that the starlight wavelength must be known $\delta\lambda \sim 0.1$ nm. It's worth noting, for context, that DCR is a major problem for all ground based astrometry (cf. Monet et al., 1992).

Fortunately, the beam combiner will usually include at least a low resolution spectrometer. In principle, with 10 nm spectral channels, the change in effective wavelength for a change in stellar temperature from 5000 to 6000 K is $\sim$0.001 nm, much better than required. In addition, absolute calibration is not required. Thus the practical requirement is on spectrometer stability: the spectrometer must be stable to $\sim$0.1 nm, i.e., to $\sim$1% of the assumed channel width, over a switching cycle. This is also challenging, but more achievable than absolute wavelength knowledge. To achieve the requirement requires a stable camera design and environment, and most likely a single-mode fiber feed to ensure a stable MTF. However, likely equally essential, is a fast-switching observational scenario to reduce the time scale for spectrometer stability and to allow averaging of errors over multiple cycles.

2.2.5 Environmental stability

As the metrology and starlight will typically be at different wavelengths, stability of the dispersive interferometer environment is also important. For metrology at 1.3 μm and starlight at 2.2 μm, the difference in dry air refractivity at

1 atmosphere is 0.6×10^{-6}. Dry air refractivity is dependent on inverse (absolute) temperature, so the temperature dependence is 2×10^{-9} K^{-1}, or 200 nm K^{-1} for a 100 m pathlength. You can do a similar calculation for changes in relative humidity, yielding 80 nm per percent change in relative humidity (Colavita et al., 2004). Note that these effects are considerably larger with HeNe (633 nm) metrology, with values of 1200 nm K^{-1} for temperature and 150 nm $\%^{-1}$ for the two terms.

These numbers are again tight compared with the 5 nm allocation for all measurement errors. However, this is a conservative analysis, not only because the path may actually be less than 100 m if one observes close to zenith and also accounts for the reduced atmospheric pressure at an observatory, but primarily because the light from the two stars is likely traversing a similar environment in the lab, i.e., the beams are likely side-by-side, ten's of cm apart. In this case, most of the error, except over the ∼10 mm OPD difference between stars, drops out, leaving only variations over 10 cm scales which should rapidly average out. In addition, a fast-switching scenario also greatly reduces stability requirements for this term, too.

2.3 Fringe measurement noise

Fringe measurement noise $\delta\phi$ refers to errors in measuring the residual fringe phase, which is used to correct the OPD measurement described above. We had allocated 5 nm to this term above.

Absent camera stability, which we discussed above, if you work at null (i.e., $\phi = 0$) there are no errors in this category; of course you won't be working exactly at null. One significant effect is that even if your phase referencing were perfect, there would still be group delay fluctuations due to water vapor turbulence as well as to the increase in dry-air path with earth rotation, as illustrated (Akeson, Swain, & Colavita, 2000; Colavita et al., 2004) in Fig. 7. In principle, group-delay feedforward to an atmospheric dispersion compensator (ADC) from the phase reference combiner could be used to reduce the size of the fluctuations, somewhat analogous to the dispersion control used for the KI nuller (Colavita et al., 2008).

Without dispersion control, to first order you need accuracy from the fringe engine of 5 nm over a range of 2.2 μm from all effects. This accuracy must also apply in the presence of small rates due to tracking errors. The sources of error include wavelength calibration, finite coherence (largely addressed with a spectrometer), and phase measurement linearity, including linearity of OPD modulation. The needed total accuracy is 0.2%, which should be achievable with care. Note that this is a place where a slow dither could be useful to

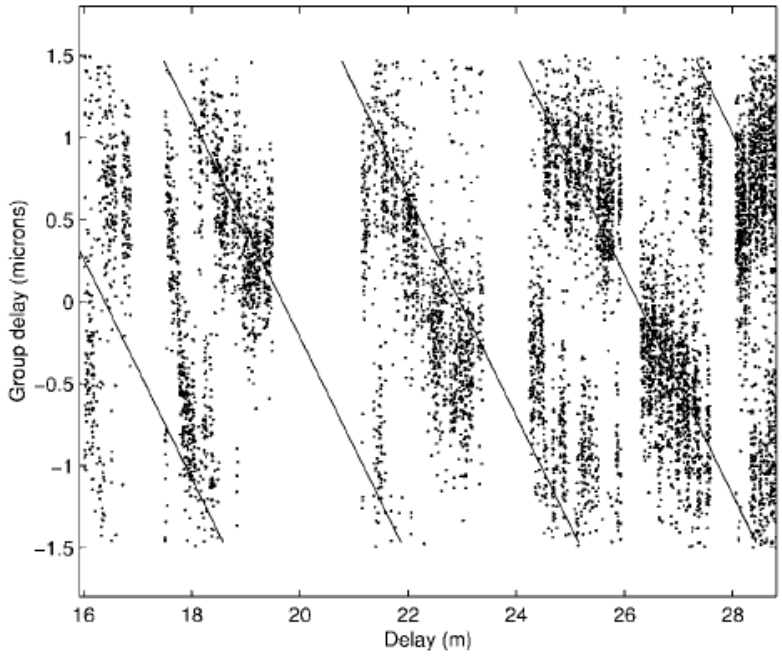

Figure 7. Group delay minus phase delay vs. total delay at PTI (adapted from Akeson et al. 2000).

provide some degree of cyclic averaging.

2.4 Summary: systematic errors

Controlling the systematic errors associated with interferometer baseline, OPD measurement, and fringe measurements is challenging and must be addressed deliberately. In particular, identification of the narrow-angle baseline is a unique problem for astrometry with a star separator. The fact that we are making a differential measurement is very useful for reducing the effect of certain error sources, as is the ability to devise an observational scenario which uses a fast-switching approach.

Figure 8 shows raw data from the PTI dual-star astrometry experiment (Lane et al., 2000). For this experiment, the first beam combiner always tracked one of the two stars. The second beam combiner rapidly switched, with a cycle time <10 min, between the two stars, and that OPD is shown in the figure. The metric for level-2 processing was the difference between the secondary star measurements and an interpolated reference from the primary star. Several metrology discontinuities are evident in the data; however, with the fast switching approach, they affect at most one 6 min data segment. More generally, only deviations from a linear trend over the switching cycle introduce

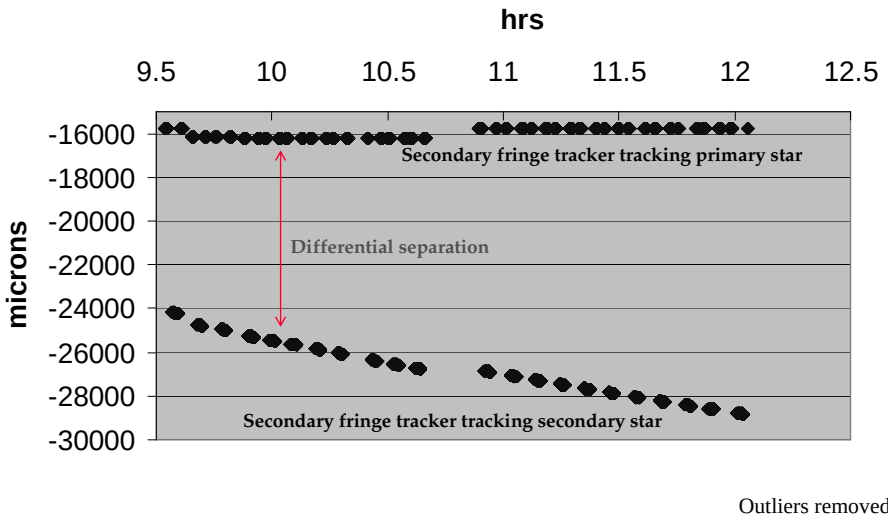

Figure 8. Raw OPD from PTI dual-star experiment.

astrometric errors.

3 Sensitivity

The squared phase SNR is given by the usual formula (cf. Colavita et al., 1999)

$$\mathrm{SNR}^2 = \frac{4}{\pi^2} \frac{N^2 V^2}{N + G + 4R} \tag{9}$$

which assumes a 4-bin algorithm, and where N is total detected photons (both apertures), V is fringe visibility, G is background photons, and R is detector read noise variance. The astrometric error e is given by

$$e = \frac{\lambda}{2\pi B \mathrm{SNR}} \tag{10}$$

For $\lambda = 2.2$ μm and $B = 100$ m, 20 μas astrometry requires an SNR of 36 (this is for the faint star: the astrometric error on the bright star should be negligible). Because of the narrow fields of view in a dual-star measurement, attention must be paid to maintaining a high SNR. This includes not only maximizing throughput, N, but also maximizing the coherence term V^2.

Assuming a single-mode combiner and incident flux F, the number of detected photons is $N = \alpha SF$, where α is the effective instrument throughput, including warm and cold loss, mode matching, detector encircled energy, read-out duty cycle, etc. The Strehl S is the product of the three terms below.

3.1.1 Beam train Strehl, S_b

For 100 nm rms per arm, and a science wavelength of 2.2 μm, this term is S_b ~90%, and should not dominate the throughput.

3.1.2 Residual wavefront error after correction, S_w.

For a small telescope, tip/tilt correction may be adequate for infrared wavelengths under good seeing conditions; here is a rough numerical example. For Kolmogorov turbulence, if you fully correct the tilt error, the wavefront variance decreases from $1.03(D/r_0)^{5/3}$ to $0.134(D/r_0)^{5/3}$ rad^2 (Noll, 1976). In reality, some tilt residual will remain, attributable to coma anisoplanatism (sensing tilt using a centroid rather than a wavefront sensor), finite temporal sampling and servo bandwidth, and sensor noise. If you assume the residual of these three effects is 5% of the variance of the tilt component, then for D = 1.8 m and r_0 = 15 cm, the rms residual is 300 nm, and Strehl $S_w \sim 50\%$ at 2.2 μm; the value degrades rapidly with poorer seeing. With higher-order correction, say from a low-order curvature system, considerably better performance is possible. This is a somewhat simplistic analysis: the main point is that finite Strehl decreases effective throughput.

3.1.3 Anisoplanatism error from off-axis wavefront correction, S_a

As the faint star will be off-axis from the bright star used for tilt correction, there will be a tilt isoplanatism error. We can estimate the Strehl from tilt errors as Alloin & Mariotti (1994): $S = 1/(1 + \sigma^2_{\rm TILT})$, where $\sigma^2_{\rm TILT} = 2\sigma_1^2/(0.637\lambda/D)^2$, and σ_1 is the one-axis tilt error. The tilt anisoplanatism error is very site- and seeing-dependent, and is also a function of the telescope diameter (Hardy, 1998). Assuming [1] a very approximate value $\sigma_1 = 0.35$ μrad at 15 arcsec off-axis, $S_a = 70\%$. Again, this is a somewhat simplistic analysis, and is again to emphasize the effect of finite Strehl.

[1] We estimate using Fig. 7.38 in Hardy (1998), multiplying by two to convert the result from a 4 arcsec visible isoplanatic patch to more typical 2 arcsec.

The coherence term V^2 in Eq. 9 includes (multiplicative) contributions from atmospheric anisoplanatism, imperfect cophasing, and residual instrumental effects, as described below.

3.2.1 Isopistonic angle

Anisoplanatism between the phase reference star and the target star reduces fringe visibility, reducing sensitivity. We compute the coherence loss using the usual Marechal approximation as $V^2 = \exp(-\sigma^2)$. In the limit of point apertures, infinite baseline, and infinite outer scale, the residual variance is given by (cf. Roddier, Gilli, & Vernin, 1982) $\sigma^2 = 2(\theta/\theta_0)^{5/3}$ rad^2, where θ_0 is the isoplanatic angle $\theta_0 = 0.31 r_0/h_{5/3}$. However, this formula overestimates the coherence loss for finite apertures and realistic baseline and outer scale assumptions. In this context, the coherence term is usually described in terms of the isopistonic angle (Esposito, Riccardi, & Femenia, 2000), which is sometimes normalized to $\lambda/10$ rms, vs. 1 radian rms for isoplanatic angle. Esposito, Riccardi, & Femenia (2000) estimate the $\lambda/10$ isopistonic angle for a VLT unit telescope as $\theta_p = 16.1$ arcsec at 2.2 μm, with a variance dependence for the error $\sigma^2 \propto (\theta/\theta_p)^2$. No value is given for an AT, but it will be smaller for a smaller telescope; roughly scaling from the UT value we estimate $\sim$10 arcsec; clearly all values are strongly site- and seeing-dependent. For this value, the coherence at a typical 15 arcsec star separation is $V^2 \approx 40\%$. This term is thus one of the larger contributors to the total SNR, and actual dual-star measurements at the site are clearly needed.

3.2.2 Cophasing time delay & instrument vibrations

In principle, this term is given by $\sigma^2 = (T_d/\tau_{02})^{5/3}$ where T_d is the end-to-end cophasing time delay and τ_{02} is the two-aperture first-difference coherence time (Buscher, 1994), (Colavita et al., 1999). The time delay depends upon the integration time on the bright star as well as the overall control architecture. However, residual instrument vibrations also contribute. Adopting 200 nm rms, based on achieved performance with the KI nuller cophasing system (Colavita et al., 2008) yields a coherence term of $V^2 = 70\%$. Clearly, optimization of this system is important.

3.2.3 Instrument coherence loss

This catch-all term encompasses those quasistatic terms that contribute to a non-unit visibility on an unresolved bright star observed at the maximum

frame rate: we would expect $V^2 = 80$–90%.

3.3 Summary: sensitivity

For the faint star at K band, note that the background term, which is traditionally ignored for bright-star interferometry, can dominate the denominator of Eq. 9. In addition, the read noise term can also be significant, as the detector must be read out fast enough to perform at least some low-bandwidth fringe tracking.

A detailed throughput calculation is beyond the current scope. However, there are some points to emphasize. The first is that, without care, SNR can dominate over the other terms. Thus, it's important to optimize those instrument factors that affect throughput, Strehl, and coherence; clearly, there's less that one can do about the fundamental atmospheric coherence terms. To further improve SNR, one could consider simultaneous K- and H-band observations; this would require incorporation of an ADC into the system, but that might be driven by other considerations. The second point is the big improvement with baseline: with a baseline of 200 m, vs. the nominal 100 m assumed above, you need $\frac{1}{2}$ the SNR, or $\frac{1}{4}$ the integration time, to achieve the same astrometric performance.

4 Conclusions

This article has primarily addressed dual-star interferometry for astrometry. However, the technique is also well suited for imaging. For imaging, most of the systematic effects in Sec. 2 don't matter as much; however, all of the SNR issues remain relevant. Some things to consider for imaging applications: a) cophasing implementation: feedback vs. feedforward, and performance with instrument vibrations; b) water-vapor dispersion: if the reference and science wavelengths are different, this needs to be accounted for; c) correlation of phase-referencing light with the science light (dispersion, metrology, etc.); d) practical issues: acquiring faint stars, providing some control bandwidth on the faint star, and optimizing the observing sequence.

In conclusion, astrometry at ten's of microarcseconds is allowed through the terrestrial atmosphere for a long-baseline dual-star interferometer. However, the fundamental atmospheric limit is only one part of a total instrument performance budget. Careful control of systematics is required, for the astrometric baseline, and for internal OPD and fringe measurements. Note in particular that the astrometric baseline for narrow-angle astrometry is generally different

than the usual wide-angle baseline. Beyond systematics, it's important to pay attention to SNR in order to optimize performance on faint stars: high SNR also just makes the measurements easier and faster.

Some approaches for systematic control and optimization of SNR were described; better approaches are surely possible. However, a couple of generally powerful approaches should be part of any implementation: a fast switching architecture, to minimize the time scale over which stability is required, and use of the longest baseline possible, limited by resolution of the target star, to exploit the inverse dependence on baseline of all of the error terms.

5 Acknowledgments

This work was performed at the Jet Propulsion Laboratory, California Institute of Technology, under contract with National Aeronautics and Space Administration.

A Beamwalk formulae

A.1 Definitions

Let Z^*, D^*, d^*, and Δ^* be respectively the physical size of the optic, the diameter of the starlight footprint, the diameter of the metrology footprint, and the beam shear. In the equations below, we use normalized values $D = D^*/Z^*$, $d = d^*/Z^*$, and $\Delta = \Delta^*/Z^*$. Let ϵ be the beam walk error.

A.2 Mirror power spectrum

Model a radial slice through the two-dimensional wavefront power spectrum (i.e., typically 4X the surface power spectrum for a normal-incidence reflection) as

$$W(f) = k^2 f^{-\alpha}, f > f_c, \tag{A.1}$$

where f is spatial frequency in cycles across the optic, $-\alpha$ is the power law obeyed by the wavefront error at high frequencies, and f_c is a cutoff frequency used for normalization. Let w^2 be the total wavefront variance over the optic.

If we arbitrarily define f_c such that 1/2 of the wavefront variance is above that frequency, i.e.,

$$w^2/2 = 2\pi \int_{f_c}^{\infty} f \mathrm{d}f W(f), \tag{A.2}$$

then the scale factor k is given by

$$k^2 = \frac{\alpha - 2}{4\pi} f_c^{\alpha-2} w^2. \tag{A.3}$$

For $f_c = 1$ cycle and assumed spectral slope of $\alpha = 2.5$,

$$k^2 = w^2/(8\pi). \tag{A.4}$$

If a power spectrum valid to zero frequency is needed, one could adopt a power law $-\alpha = -1.5$ for $f_c < 1$, which provides equal total power below 1 cycle as above.

A.3 Filter functions

A.3.1 Simple shear of two equal-size beams

We can write the error variance as

$$\epsilon^2 = \langle \left| \frac{1}{A} \int \mathrm{d}\mathbf{r} x(\mathbf{r}) - \frac{1}{A} \int \mathrm{d}\mathbf{r} x(\mathbf{r} - \mathbf{\Delta}) \right|^2 \rangle \tag{A.5}$$

where $x(\mathbf{r})$ is the wavefront defined over a pupil function. We can represent the random function $x(\mathbf{r})$ using a Fourier-Stieltjes integral,

$$x(\mathbf{r}) = \int dW(\mathbf{f}) \exp\left(-j2\pi \mathbf{f} \cdot \mathbf{r}\right), \tag{A.6}$$

and use the Fourier shift theorem to write

$$\epsilon^2 = \langle \left| \int \mathrm{d}W(\mathbf{f})(1 - \exp(-j2\pi \mathbf{f} \cdot \mathbf{\Delta})) \frac{1}{A} \int \mathrm{d}\mathbf{r} \exp(-j2\pi \mathbf{f} \cdot \mathbf{r}) \right|^2 \rangle. \tag{A.7}$$

Computing the second integral yields

$$\epsilon^2 = \langle \left| \int \mathrm{d}W(\mathbf{f})(1 - \exp(-j2\pi \mathbf{f} \cdot \mathbf{\Delta})) \left(\frac{2J_1(\pi f D)}{\pi f D} \right) \right|^2 \rangle \tag{A.8}$$

Expanding this expression, and applying the Fourier-Stieltjes sifting property,

$$\left\langle \int\int dW(\mathbf{f})dW^*(\mathbf{g}) \right\rangle = \int\int \mathrm{d}\mathbf{f}\mathrm{d}\mathbf{g}W(\mathbf{f})\delta(\mathbf{f}-\mathbf{g}), \tag{A.9}$$

yields

$$\epsilon^2 = \int \mathrm{d}fW(\mathbf{f})2(1-\cos(2\pi\mathbf{f}\cdot\mathbf{\Delta}))\left(\frac{2J_1(\pi fD)}{\pi fD}\right)^2. \tag{A.10}$$

Finally, we compute the azimuthal part of the first integral to yield

$$\epsilon^2 = 2\pi\int f\mathrm{d}fW(f)2(1-J_0(2\pi f\Delta))\left(\frac{2J_1(\pi fD)}{\pi fD}\right)^2. \tag{A.11}$$

In general, these results have a common form:

$$\epsilon^2 = 2\pi\int f\mathrm{d}fW(f)H(f), \tag{A.12}$$

where $W(f)$ is the mirror power spectrum and $H(f)$ is a filter function; in this case:

$$H_1(f) = 2(1-J_0(2\pi f\Delta))\left(\frac{2J_1(\pi fD)}{\pi fD}\right)^2. \tag{A.13}$$

For $\Delta \ll D$, we can approximate the second factor of $H_1(f)$ as unity to $f = 1/D$ and zero at higher frequencies, and the first factor as $2(\pi f\Delta)^2$. Let $W(f) = k^2 f^{-2.5}$, as above, and for $D \ll 1$, assume it is valid to zero frequency (it gets rolled off by the $(\pi f\Delta)^2$ factor), and approximate the error integral as

$$\epsilon^2 \simeq 4\pi\int_0^{1/D} \mathrm{d}fk^2 f^{-1.5}(2\Delta f)^2, \tag{A.14}$$

showing that most of the energy is from frequencies $\sim 1/D$. Doing the error integral without the approximations to the Bessel functions to accurately compute the leading coefficient yields

$$\epsilon^2 \simeq 37k^2\Delta^2 D^{-1.5}, \Delta \ll D, \tag{A.15}$$

or with k as defined above,

$$\epsilon^2 \simeq 1.5w^2\Delta^2 D^{-1.5}, \Delta \ll D. \tag{A.16}$$

This result is a bit pessimistic as D approaches unity because of the low-frequency power law assumption above. A numerical integration for $D = 1$ assuming $\alpha = 1.5$ at low frequencies, as described above, gives a factor of two smaller variance. The next term in the expansion of the first factor of $H_1(f)$ is $0.5(\pi f \Delta)^4$, which leads to variance terms proportional to $\Delta^4 D^{-3.5}$, which should be negligible given all of the other assumptions involved.

A.3.2 Change in metrology distance vs. starlight distance as beam shears

The error can be written as

$$\epsilon = \langle \left| \left(\frac{1}{A} \int \mathrm{d}\mathbf{r} x(\mathbf{r}) - \frac{1}{a} \int \mathrm{d}\mathbf{r} x(\mathbf{r}) \right) - \left(\frac{1}{A} \int \mathrm{d}\mathbf{r} x(\mathbf{r} - \boldsymbol{\Delta}) - \frac{1}{a} \int \mathrm{d}\mathbf{r} x(\mathbf{r} - \boldsymbol{\Delta}) \right) \right|^2 \rangle, \quad \text{(A.17)}$$

which leads to a filter function

$$H_2(f) = 2(1 - J_0(2\pi f \Delta)) \left(\frac{2J_1(\pi f D)}{\pi f D} - \frac{2J_1(\pi f d)}{\pi f d} \right)^2. \quad \text{(A.18)}$$

We can approximate the error for the assumed power spectrum and $2\Delta \ll d \ll D$ as

$$\epsilon^2 \simeq 4\pi \int_0^{1/d} \mathrm{d}f k^2 f^{-1.5} (2\Delta f)^2, \quad \text{(A.19)}$$

which gives a similar result as above:

$$\epsilon^2 \simeq 37 k^2 \Delta^2 d^{-1.5}, 2\Delta \ll d \ll D, \quad \text{(A.20)}$$

or with k as defined above:

$$\epsilon^2 \simeq 1.5 w^2 \Delta^2 d^{-1.5}, 2\Delta \ll d \ll D. \quad \text{(A.21)}$$

For $d \ll 2\Delta \ll D$, we can approximate the error as

$$\epsilon^2 \simeq 4\pi \int_0^{1/(2\Delta)} \mathrm{d}f k^2 f^{-1.5} (2\Delta f)^2, \quad \text{(A.22)}$$

which leads to (doing the numerical integral to compute the leading coefficient)

$$\epsilon^2 \simeq 56 k^2 \Delta^{0.5}, d \ll 2\Delta \ll D, \quad \text{(A.23)}$$

or with k as defined above,

$$\epsilon^2 \simeq 2.2w^2\Delta^{0.5}, d \ll 2\Delta \ll D. \tag{A.24}$$

For higher accuracy within the limitations of the model, it's probably best to just compute the integral using $H_2(f)$.

A.3.3 Simple shear of two equal-size Gaussian beams

Let the Gaussian beam radius (amplitude 1/e) be R. The filter function is then

$$H_3(f) = 2(1 - J_0(2\pi f\Delta)) \exp(-2(\pi f R)^2). \tag{A.25}$$

Calculating asymptotic forms as above yields

$$\epsilon^2 \simeq 8.1k^2\Delta^2 R^{-1.5}, \Delta \ll R, \tag{A.26}$$

or with k as defined above,

$$\epsilon^2 \simeq 0.32w^2\Delta^2 R^{-1.5}, \Delta \ll R. \tag{A.27}$$

A.3.4 Other filter functions

Analogous to the pencil-beam / full-aperture-beam expression above, except for Gaussian beams of radii R and r, the filter function is

$$H_4(f) = 2(1 - J_0(2\pi f\Delta)) \left(\exp(-(\pi f R)^2) - \exp(-(\pi f r)^2)\right)^2. \tag{A.28}$$

For the case of a Gaussian metrology beam only, the filter function is

$$H_5(f) = 2(1 - J_0(2\pi f\Delta)) \left(\frac{2J_1(\pi f D)}{\pi f D} - \exp(-(\pi f r)^2)\right)^2. \tag{A.29}$$

References

Akeson, R. L., Swain, M. R., & Colavita, M. M., 2000, Proc. SPIE, 4006, 321

Alloin, D. M. & Mariotti, J.-M., 1994, Adaptive Optics for Astronomy, Springer, Berlin

Buscher, D. F., 1994, Proc. SPIE, 2200, 260

Ciddor, P. E., 1996, Appl. Opt., 35, 1566
Colavita, M. M., Wallace, J. K., Hines, B. E., et al., 1999, ApJ, 510, 505
Colavita, M. M., Swain, M. R., Akeson, R. L., Koresko, C. D., Hill, R. J., 2004, PASP, 116, 876
Colavita, M. M., Serabyn, E., Booth, A. J., et al., 2008, Proc. SPIE 7013, 70130A
Esposito, S., Riccardi, A., & Femenia, B., 2000, A&A, 353, L29
Hardy, J. W., 1998, Adaptive Optics for Astronomical Telescopes, Oxford Univ. Press, Oxford
Hrynevych, M. A., Ligon, E. R., & Colavita, M. M., 2004, Proc. SPIE, 5491, 1649
Lane, B. F., Colavita, M. M., Boden, A. F., & Lawson, P. R., 2000, Proc. SPIE, 4006, 452
Monet, D. G., Dahn, C. C., Vrba, F. J., et al., 1992, AJ, 103, 638
Noll, R. J., 1976, J. Opt. Soc. Am, 66, 207
Perryman, M. A. C., Lindegren, L., Kovalevsky, et al., 1997, A&A, 323, L49
Roddier, F., 1981, in Progress in Optics, XIX, E. Wolf, ed. North-Holland, 281
Roddier, F., Gilli, J. M., & Vernin, J., 1982, J. Optics (Paris), 13, 63
Shao, M. & Colavita, M. M., 1992, A&A, 262, 353
Zacharias, N., Gaume, R., Dorlan, B., & Urban, S. E., 2004, "Catalog Information and Recommendations," http://ad.usno.navy.mil/star/star_cats_rec.shtml#hip